Supporting Information

Bosmans et al. 10.1073/pnas.1108497108

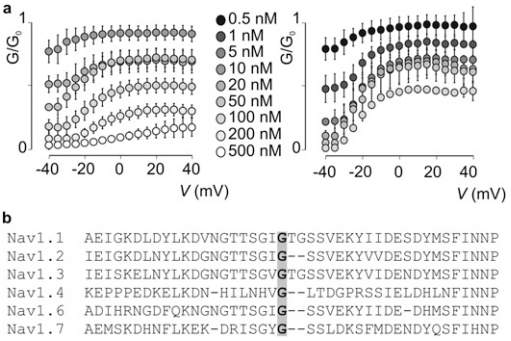

Fig. S1. Apparent affinity measurement of PaurTx3 for rNav1.2a and G1079C. (*A*) Voltage-dependent inhibition of rNav1.2a (*Left*) and the mutant channel (*Right*) by PaurTx3 over a range of concentrations. G/G_0 is the fraction of uninhibited current elicited by a depolarization to the indicated voltages (*V*). The values of G/G_0 measured in the plateau phase at negative voltages where toxin-bound channels do not open were taken as the fraction unbound (Fu). (*B*) Sequence alignment of a portion of the domain II-domain III intracellular loop of various Nav channel isoforms. Conserved glycines are highlighted by a gray background.

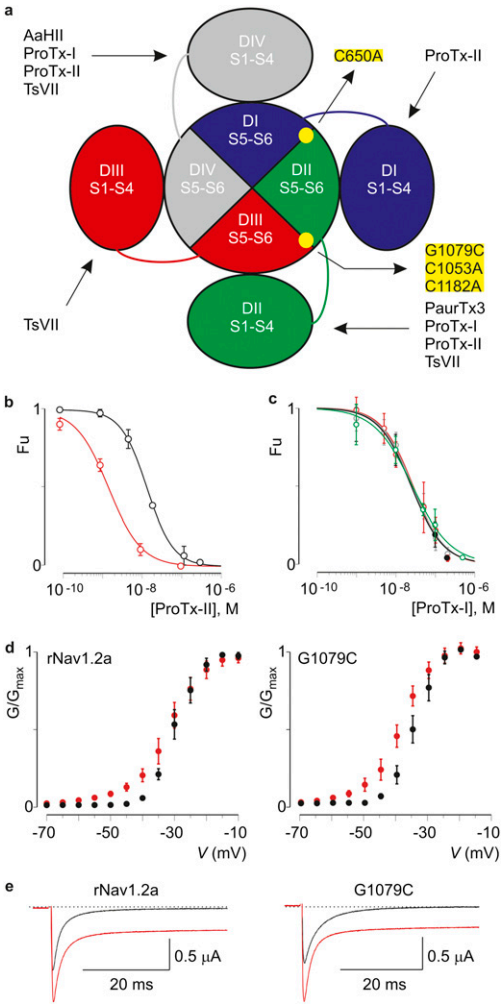

Fig. S2. Apparent affinity of voltage sensor toxins for rNav1.2a and G1079C. (*A*) Yellow dots on the Nav channel cartoon indicate the putative locations of the mutants reported here. Voltage sensors targeted by PaurTx3, ProTx-I, ProTx-II, TsVII, and AaHII also are indicated. (*B*) Apparent affinity for ProTx-II interacting with wt rNav1.2a (black) and the G1079C mutant (red). (*C*) Apparent affinity of ProTx-I interacting with wt rNav1.2a (black) and the G1079C mutant (green) after channel depalmitoylation. Data are compared with rNav1.2a (gray) and G1079C (red) before addition of 2-Br-palmitate. Concentration dependence for toxin inhibition plotted as Fu measured at negative voltages is shown. $n = 3–4$ for each toxin concentration, and error bars represent SEM. (*D*) Effect of 50 nM TsVII on rNav1.2a (*Left*) and G1079C (*Right*). Control data are represented in black, whereas toxin data are displayed in red. $n = 4$, and error bars represent SEM. (*E*) Effect of 10 nM AaHII on wt rNav1.2a and G1079C. Sodium currents are elicited by a depolarization to 0 mV before (black) and after (red) addition of AaHII from a holding potential of −90 mV. Values are reported in Tables S1 and S2.

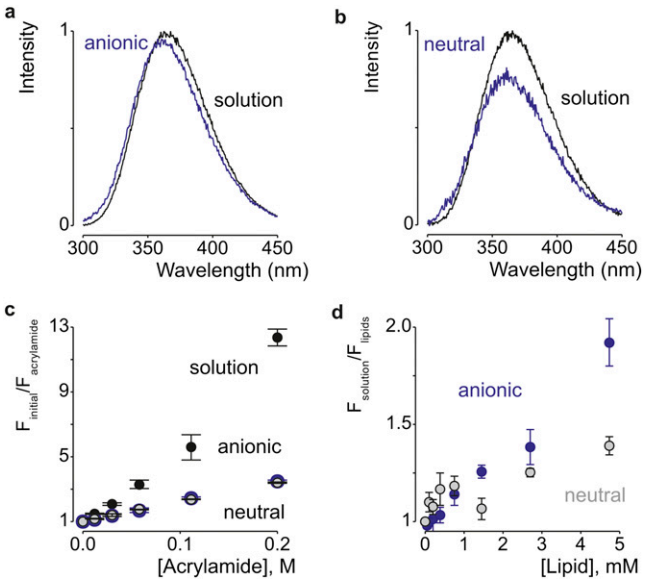

Fig. S3. Partitioning of PaurTx3 into artificial membranes. Partitioning of PaurTx3 into neutral (POPC) or anionic (1:1 mix of POPC:POPG) membranes was assayed by using tryptophan fluorescence. Fluorescence spectra for 10 μM toxins in 10 mM Hepes and 1 mM EDTA at pH 7.6 were recorded between 300 and 400 nm (5 nm band pass, 0° polarizer) by using an excitation wavelength of 280 nm (5 nm band pass, 90° polarizer) (SPEX FluoroMax 3 spectrofluorometer) and corrected for vesicle scattering. (*A* and *B*) Fluorescence emission spectra of PaurTx3 in the absence (black) or presence (blue) of 4 mM anionic (*A*) and neutral (*B*) membranes, respectively. (*C*) Stern–Volmer plots for acrylamide quenching of tryptophan fluorescence in solution (black) and in the presence of lipid membranes. Gray, neutral membranes; blue, anionic membranes. (*D*) Fluorescence intensity at 320 nm plotted as a function of available lipid concentration (60% of total lipids). $n = 3$; error bars are SEM.

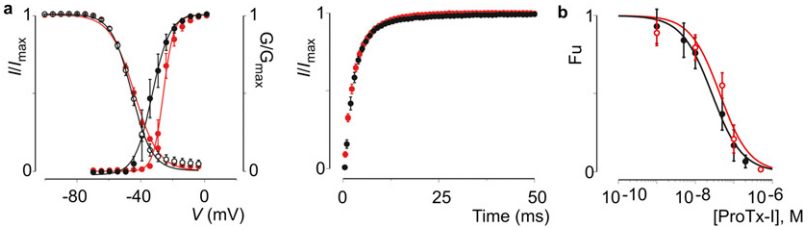

Fig. S4. Effects of cholesterol depletion on the gating properties of G1079C. (*A*) Deduced conductance–voltage and steady-state inactivation relationships (*Left*) and recovery from inactivation (*Right*) before (black) and after (red) 5 mM methyl-β-cyclodextrin are shown. (*B*) Apparent affinity of ProTx-I interacting with G1079C before (black) and after (red) membrane cholesterol depletion. Concentration dependence for toxin inhibition plotted as Fu measured at negative voltages is shown. Solid line represents a fit with the Hill equation. $n = 3$, and error bars represent SEM.

Table S1. Gating characteristics of rNav1.2a and G1079C before and after depalmitoylation

	rNav1.2a	G1079C
Before depalmitoylation		
Activation, $V_{1/2}$	−24.3 ± 0.6 mV	−33.6 ± 0.3 mV
Inactivation, $V_{1/2}$	−44.8 ± 0.5 mV	−46.2 ± 0.2 mV
Recovery, τ	5.0 ± 0.1 ms	3.3 ± 0.1 ms
After depalmitoylation		
Activation, $V_{1/2}$	−24.2 ± 0.3 mV	−28.3 ± 0.5 mV
Inactivation, $V_{1/2}$	−55.2 ± 0.5 mV	−55.6 ± 0.4 mV
Recovery, τ	13.2 ± 0.1 ms	12.8 ± 0.1 ms

Values were obtained by fitting data with single Boltzmann functions ($V_{1/2}$) or a single exponential function (τ).

Table S2. Apparent affinity values for toxins interacting with rNav1.2a and G1079C in control membranes and after 2-Br-palmitate addition obtained using the Hill equation

	rNav1.2a	G1079C
Before 2-Br-palmitate addition		
PaurTx3	27 ± 2 nM (n = 1.2 ± 0.1)	1 ± 1 nM (n = 1.0 ± 0.2)
ProTx-II	15 ± 1 nM (n = 1.3 ± 0.1)	2 ± 1 nM (n = 1.1 ± 0.1)
ProTx-I	27 ± 3 nM (n = 1.1 ± 0.1)	26 ± 3 nM (n = 1.1 ± 0.1)
AaHII	4 ± 1 nM (n = 1.1 ± 0.1)	3 ± 1 nM (n = 1.0 ± 0.1)
After 2-Br-palmitate addition		
PaurTx3	10 ± 1 nM (n = 1.0 ± 0.1)	9 ± 1 nM (n = 0.9 ± 0.1)
ProTx-II	3 ± 1 nM (n = 1.2 ± 0.1)	3 ± 1 nM (n = 1.0 ± 0.1)
ProTx-I	25 ± 4 nM (n = 1.1 ± 0.2)	28 ± 4 nM (n = 0.9 ± 0.1)
AaHII	3 ± 1 nM (n = 1.1 ± 0.1)	5 ± 1 nM (n = 1.0 ± 0.1)

Hill coefficients (n) are given in parentheses.

Table S3. Gating characteristics comparison of rNav1.2a, rNav1.2a^{AAA}, and C1182A before and after depalmitoylation

	rNav1.2a	rNav1.2a^{AAA}	C1182A
Before depalmitoylation			
Activation, $V_{1/2}$	−24.3 ± 0.6 mV	−35.6 ± 0.3 mV	−31.7 ± 0.1 mV
Inactivation, $V_{1/2}$	−44.8 ± 0.5 mV	−57.6 ± 0.3 mV	−53.5 ± 0.2 mV
Recovery, τ	5.0 ± 0.1 ms	11.2 ± 0.2 ms	7.6 ± 0.2 ms
After depalmitoylation			
Activation, $V_{1/2}$	−24.2 ± 0.3 mV	−32.8 ± 0.1 mV	−34.5 ± 0.2 mV
Inactivation, $V_{1/2}$	−55.2 ± 0.5 mV	−53.7 ± 0.3 mV	−50.8 ± 0.3 mV
Recovery, τ	13.2 ± 0.1 ms	17.9 ± 1.0 ms	14.9 ± 2.0 ms

Values were obtained by fitting data with single Boltzmann functions ($V_{1/2}$) or a single exponential function (τ).

Table S4. Apparent affinity values for toxins interacting with rNav1.2a, rNav1.2a^{AAA}, and C1182A in control membranes and after 2-Br-palmitate addition obtained using the Hill equation

	rNav1.2a	rNav1.2a^{AAA}	C1182A
PaurTx3	27 ± 2 nM (n = 1.2 ± 0.1)	5 ± 1 nM (n = 1.0 ± 0.1)	10 ± 1 nM (n = 1.0 ± 0.1)
PaurTx3*	10 ± 1 nM (n = 1.0 ± 0.1)	10 ± 1 nM (n = 1.2 ± 0.1)	6 ± 1 nM (n = 1.0 ± 0.1)

Hill coefficients (n) are given in parentheses.
*Data shown for after 2-Br-palmitate addition.